https://ntrs.nasa.gov/search.jsp?R=19790010789 2020-03-21T23:35:34+00:00Z

General Disclaimer

One or more of the Following Statements may affect this Document

- This document has been reproduced from the best copy furnished by the organizational source. It is being released in the interest of making available as much information as possible.

- This document may contain data, which exceeds the sheet parameters. It was furnished in this condition by the organizational source and is the best copy available.

- This document may contain tone-on-tone or color graphs, charts and/or pictures, which have been reproduced in black and white.

- This document is paginated as submitted by the original source.

- Portions of this document are not fully legible due to the historical nature of some of the material. However, it is the best reproduction available from the original submission.

Produced by the NASA Center for Aerospace Information (CASI)

NASA Technical Memorandum 78561

(NASA-TM-78561) EVALUATION OF A WAKE VORTEX UPSET MODEL BASED ON SIMULTANEOUS MEASUREMENTS OF WAKE VELOCITIES AND PROBE-AIRCRAFT ACCELERATIONS (NASA) 42 p HC A03/MF A01 CSCL 01C G3/03

N79-18960

Unclas 16380

Evaluation of a Wake Vortex Upset Model Based on Simultaneous Measurements of Wake Velocities and Probe-Aircraft Accelerations

Barbara J. Short and Robert A. Jacobsen

March 1979

National Aeronautics and Space Administration

NOMENCLATURE

a_n, a_y	normal and lateral accelerations at the center of gravity
b	wing span or vertical tail height
$C_{L_{\alpha_H}}$	horizontal tail lift curve slope corrected for downwash angle
$C_{L_{\alpha_i}}$	wing section lift curve slope at strip i
C_ℓ, C_m, C_n	rolling, pitching, and yawing moment coefficients
C_{m_o}	pitching moment coefficient at zero angle of attack
C_{N_α}, C_{Y_β}	normal and lateral force curve slopes
$C_{Y_{\beta_T}}$	vertical tail-lateral force curve slope corrected for sidewash angle
c	mean wing chord
c_R, c_T	root and tip chords
d	half the distance between left and right vortices
d_1, d_2	vertical locations of left and right vortices
h_1, h_2	lateral locations of left and right vortices
I_x, I_y, I_z	moments of inertia about the aircraft body axes
i	strip number
M_{α_F}, N_{β_F}	estimated fuselage pitching and yawing moment parameters
p, q, r	angular velocities about the aircraft body axes
$\dot{p}$, $\dot{q}$, $\dot{r}$	measured angular accelerations
$\dot{p}_v$, $\dot{q}_v$, $\dot{r}_v$	vortex-induced angular accelerations
$\dot{p}_{v_{meas}}$, $\dot{p}_{v_{pred}}$	measured and predicted peak roll accelerations
$\bar{q}$	dynamic pressure
r_1, r_2	distances to the left and right vortices in the vortex-axes system
S	wing reference area

PRECEDING PAGE BLANK NOT FILMED

S_i, S_o	area of strip i and initial value used in strip theory geometry
T	transformation matrix from body-axes system to vortex-axes system
V	true airspeed
V_y, V_z	lateral and vertical components of vortex velocity in the Earth-axes system
v_i, w_i	lateral and vertical components of vortex velocity on strip i in body-axes system
v_v, w_v	lateral and vertical components of vortex velocity on strip i in vortex-axes system
W	gross weight of aircraft
x_i, y_i, z_i	body-axes coordinates of a point on strip i
x_o, y_o, z_o	initial values of coordinates in strip theory geometry
y_{cg}, z_{cg}	Earth-axes coordinates of aircraft center of gravity
y_{cg_v}, z_{cg_v}	vortex-axes coordinates of aircraft center of gravity
y_v, z_v	vortex-axes coordinates of a point on strip i
y_{v_o}, z_{v_o}	Earth-axes coordinates of vortex-axes origin
α, β	angles of attack and sideslip
α_c, β_c	effective angles of attack and sideslip at aircraft center of gravity
α_{dyn}, β_{dyn}	dynamic angles of attack and sideslip
α_F, β_F	fuselage incremental angles of attack and sideslip
α_i, β_i	incremental angles of attack and sideslip at strip i
α_{IC}, β_{IC}	initial angles of attack and sideslip prior to vortex encounter
α_{max}, β_{max}	maximum angles of attack and sideslip
α_{min}, β_{min}	minimum angles of attack and sideslip
β_v	vortex core size parameter

Γ	vortex circulation
ΔS	incremental area used in strip theory geometry
Δx, Δy, Δz	increments in coordinates used in strip theory geometry
δ_a, δ_e, δ_r	aileron, elevator, and rudder deflection angles
λ	angle of sweep
μ	orientation of vortex axes in Earth-axes system
ψ, θ, ϕ	Euler angles of aircraft with respect to inertial space

Subscripts

LHT, RHT	left and right horizontal tail
LW, RW	left and right wing
p	partial derivative with respect to $\frac{pb}{2V}$
q	partial derivative with respect to $\frac{qc}{2V}$
r	partial derivative with respect to $\frac{rb}{2V}$
VT	vertical tail
α	partial derivative with respect to α
β	partial derivative with respect to β
δ_a	partial derivative with respect to δ_a
δ_e	partial derivative with respect to δ_e
δ_r	partial derivative with respect to δ_r

EVALUATION OF A WAKE VORTEX UPSET MODEL BASED ON SIMULTANEOUS MEASUREMENTS OF WAKE VELOCITIES AND PROBE-AIRCRAFT ACCELERATIONS

Barbara J. Short and Robert A. Jacobsen

Ames Research Center

SUMMARY

Simultaneous measurements have been made of the upset responses experienced and the wake velocities encountered by an instrumented Learjet probe aircraft behind a Boeing 747 vortex-generating aircraft. The vortex-induced angular accelerations experienced could be predicted within 30% by a mathematical upset response model when the characteristics of the wake were well represented by the vortex model. The vortex model used in the present study adequately represented the wake flow field when the vortices dissipated symmetrically and only one vortex pair existed in the wake.

INTRODUCTION

The third generation air traffic control system proposed for the 1980's by the Federal Aviation Administration is based, in part, on an increased rate of terminal area operations (ref. 1). This would require a reduction in the minimum separation distance between aircraft on their approach and departure. The minimum separation distance is currently limited by the hazards associated with wake vortex encounters. Two approaches to solving the wake vortex problem have been the subjects of intensive research programs. One approach is to develop a wake vortex avoidance system for the terminal airspace, which has been under study by the U.S. Department of Transportation (refs. 2-6). The other approach to the wake vortex problem is to develop an aerodynamic means to reduce the hazard associated with a wake encounter. This approach has been the subject of a NASA research program for several years (refs. 7-17). A number of vortex hazard alleviation techniques have been developed in NASA ground-based facilities, and several have shown sufficient promise to warrant evaluation in flight.

Two flight test techniques have been employed to evaluate the severity of wake vortex encounters and the effectiveness of aerodynamic alleviation techniques. The oldest and most frequently used approach is to measure the accelerations imparted to an aircraft penetrating the vortex wake at a known separation from the generating aircraft. This technique requires a minimum of instrumentation and data reduction. However, there are several disadvantages to this technique. First, even though the wake has been made visible by one of several available methods, it is difficult to penetrate its center to achieve the maximum upset. Therefore, unless a large number of encounters are made, it is difficult to assure that the maximum possible wake severity has been recorded. Second, and equally important, extrapolation of results to

other penetrating aircraft cannot be accomplished with confidence because the upsetting moment depends on the vortex characteristics and varies nonlinearly with the span of the penetrating aircraft.

An alternative flight test technique is to measure the velocities in the wake and infer the entire wake vortex flow field through matching a mathematical vortex model to the measurements. If this can be done, then computations can be made of the aerodynamic forces and moments imparted to arbitrary following aircraft. This requires that an adequate vortex model be available that can be successfully inferred from the measured velocities and that a suitable computational method be available for estimating the forces and moments resulting from the vortex.

A technique of inferring the wake vortex flow field from inflight velocity measurements has been described in reference 18. A mathematical model based on simple strip theory has been used by several investigators to estimate vortex-induced forces and moments (refs. 19-24), but little has been done to verify or refine those models. One of the reasons for this is that an adequate set of data by which models can be judged has not been available. Recently, a flight test program at NASA's Dryden Flight Research Center to investigate the use of wing spoilers for attenuation of the vortices from a Boeing 747 provided an opportunity for the measurement of the upset of an aircraft simultaneously with measurements of the wake vortex velocities. This was possible through the use of the instrumented Learjet operated by NASA's Ames Research Center. The results of these simultaneous measurements along with the development of an impr ed mathematical model for estimation of vortex-induced moments are presented herein.

TEST DESCRIPTION

Test Aircraft

The Boeing 747 aircraft (fig. 1) used as a wake generating airplane for this investigation was modified to allow the wing spoiler panels to be deployed independently. Smoke generators were mounted on each wing tip, at the outboard edge of the outboard flap segment, and at the outboard edge of the inboard flap segment. A modified Distance Measuring Equipment (DME) unit was installed in the aircraft to allow direct measurement of the range to probe aircraft. A physical description of the Boeing 747 is given in table 1.

The Learjet probe aircraft, also shown in figure 1, was instrumented to measure the parameters pertinent to upset dynamics, including the aircraft motions and its control-surface deflections. Airspeed, altitude, and angles of attack and sideslip were measured by an instrumented boom on the nose of the aircraft. A three-component hot-wire anemometer probe was also mounted on the nose boom of the aircraft for measuring velocities in the wake. The data were recorded on magnetic tape aboard the aircraft. The response measurements to document the upset resulting from an encounter were recorded in digital form, while the hot-wire anemometer measurements were recorded in

analog form because of their high-frequency content. A time base generated aboard the aircraft was recorded in both analog and digital formats to allow correlation of the flow-field measurements with the upset measurements to reduce the data. A physical description of the Learjet is given in table 1.

Test Conditions

The flight tests on the Boeing 747 were conducted at an altitude of approximately 3,040 m (10,000 ft) at airspeeds from 143 to 148 knots indicated airspeed (KIAS). The gross weight of the Boeing 747 ranged from 240,000 to 259,000 kg (530,000 to 572,000 lb). The lift coefficient was maintained at 1.4. Two configurations of the Boeing 747 were tested. The baseline configuration was the normal Boeing 747 landing configuration with both the inboard and outboard flap segments deflected 30° (flap setting, 30/30) and the wing spoilers retracted. The vortex minimization configuration investigated was one with the flap setting remaining at 30/30 but wing spoiler panels 1, 2, 11, 12 deflected 41°. The locations of these spoiler panels on the wing of the Boeing 747 are indicated in figure 2. The results of using spoilers for alleviation of the hazard associated with a vortex encounter are reported in references 8 and 25-28.

Flight Test Procedures

Two different flight test procedures are normally used to obtain the upset and velocity profile data. The major difference between the techniques is that in making measurements of the upset resulting from a vortex encounter the probe aircraft attempts to fly along a path coincident with the axis of the vortex; in making velocity profile measurements, a flight path nearly normal to the wake is desirable. To acquire velocity profile measurements and measurements of the upset resulting from the encounter, a compromise between these two techniques was required. The flight path of the Learjet was at a nominal angle of 25° to the axes of the vortices, although a few measurements were taken with angles as high as 40° and as small as 15°.

For each configuration studied, the wake is initially encountered at a separation distance which is large enough to assure safety. Data are then obtained at decreasing distances until a predetermined minimum distance is reached or until the continued reduction of separation distance is judged to be hazardous either by the pilot of the probe aircraft or through assessment of the loads imposed on the aircraft. For all of these measurements, the wake was made visible by injecting smoke into it. This provided a target for the pilot in his task. When crossing the wake, the pilot attempted to penetrate the core of one of the vortex pairs with the nose boom of the Learjet. A number of passes were made across the wake to ensure that adequate data were obtained.

Analysis Method

The signal flow diagram of figure 3 shows how the airborne data and ground processing are used to produce predicted vortex-induced angular accelerations, which are compared with the measured vortex-induced angular accelerations. The airborne data system begins with sensors to measure both the flow field in which the probe aircraft is flying and the dynamics and control inputs that are experienced by the aircraft. These data are electronically conditioned to provide signals adequate for the tape recorders. It is necessary to record the flow-field information in analog form because of the high frequency content of the desired information. The dynamics and control inputs of the probe aircraft, being of considerably lower frequency content, are recorded by a digital tape recorder after being sampled at a rate of 100 samples per second. A time signal generated on-board is recorded on both recorders simultaneously providing a way to correlate the two sets of data.

The two sets of recorded data undergo considerable processing in ground computer facilities. To develop the predicted acceleration requires processing of the flow-field information. The analog data from the airplane are digitized at a rate of 1000 samples per second to preserve their frequency content. The data are then processed to provide wake velocity information along the actual flight path of the probe aircraft. By using an iterative technique, the velocity data are matched by a mathematical model of a vortex pair. The mathematical model used is one originally derived by Sir Horace Lamb (ref. 29). Although more precise models are known (refs. 30-34), the Lamb model is expressed as a single continuous function, which simplifies the matching procedure. The parameters in the matching procedure are the vortex strength, the core size, and the positions of the two vortices in inertial space. These parameters are varied to provide the best match in a least-squares sense to vertical and lateral velocities as measured along the flight path.

The mathematical upset model (discussed in a later section of this report) uses the modeled wake as input and produces estimates of the angular accelerations that would result as the aircraft encountered the wake. These predicted accelerations are computed while constraining all other parameters of the upset model to be the same as the actual case.

To judge the adequacy of the upset model, the actual angular accelerations induced by the vortex system are computed from the measured parameters on the aircraft. Effective angles of attack and sideslip must be computed from the aircraft's linear accelerations because the vanes mounted on the nose boom respond to the flow at only one point and it is necessary to have an integrated effect over the whole aircraft. The angular accelerations resulting from the aerodynamics and control inputs are computed and then subtracted from the measured angular accelerations. This results in isolating the portion of the angular accelerations that were induced solely by the vortex flow field. The predicted vortex-induced angular accelerations are compared with those that were measured thereby providing a means of evaluating the mathematical upset model.

UPSET RESPONSE MODEL

Predicted upset responses in the form of time histories of the angular accelerations of the probe aircraft were calculated with the use of the strength, size, and location of the vortex pair determined from the velocity profile measurements. The incremental forces and moments acting on the probe aircraft during vortex encounter were calculated with the use of strip theory as discussed in references 19 and 20 and as used in simulation studies of vortex encounter hazard criteria (refs. 21-23). The equations used in the present report to predict the vortex-induced angular accelerations are presented in Appendix A.

The wing, horizontal tail, and vertical tail were divided into chordwise strips, and the vortex-induced angles of attack and sideslip were computed for each strip. The incremental forces and moments were then calculated, summed, and combined with an estimated contribution from the fuselage to produce the net roll, pitch, and yaw accelerations resulting from the vortex pair as defined by the velocity-profile model. This procedure was followed for each point along the flight path of the probe aircraft to produce time histories of the predicted accelerations.

For a comparison of predicted and measured accelerations induced by the vortices, it is necessary that the total measured accelerations be corrected for the aerodynamics that result from control surface deflections, angular rates, and attitude of the probe aircraft, as discussed in reference 18. The method used to extract the vortex-induced angular accelerations from the total measured angular accelerations is reproduced in Appendix B. The results of both the basic analysis method and of its refinements are demonstrated in figures 4 through 7. In figure 4 are presented the time histories of the vertical velocity component V_z and the lateral velocity component V_y as measured in the wake of the Boeing 747 at a separation distance of 1.7 nautical miles. The 747 was in its normal approach configuration with no spoilers deployed. The velocity components along the same flight path resulting from the two-vortex mathematical model matched to the data are shown as solid lines. In this case, the two-vortex model adequately represents the actual wake structure as measured along the flight path of the probe aircraft.

The body-axes components of the vortex-induced angular accelerations predicted by the basic upset response model, with the mathematical wake model from figure 4 as input, are presented as time histories in figure 5. The measured vortex-induced angular accelerations are also shown in figure 5 for comparison. The predicted roll accelerations are in fair agreement with the measured values as seen in the upper curve; however, the pitch and yaw accelerations (middle and lower curves, respectively) are not well predicted. The large values of predicted pitch accelerations result from the contribution of the horizontal tail. The basic upset response model assumes no change in the vortex flow field as the probe aircraft passes through it, although some attenuation of the vortex would be expected after its interaction with the wing. As a first approximation, to correct this incongruity, the contribution of the horizontal tail was removed entirely from the upset response model.

The results are shown in figure 6. The absence of vortex-induced loads on the horizontal tail markedly improves the prediction of pitch accelerations and has only a slight effect on the predicted roll and yaw acceleration. The mismatch of the yaw acceleration-time history shown here did not always occur. This can be attributed to the fact that with the mathematical model for upset responses as used in references 21-23, the aerodynamic forces were calculated with respect to a local wind-axes system at each strip, and the horizontal components were ignored in the transformation to the body-axes system. Consequently, the contribution of the chordwise component of wing lift to the yawing moment is omitted. In some cases, this contribution completely overshadows the yawing moment of the vertical tail. For the present tests, all forces and moments were calculated in the body-axes system (Appendix A). The results of that correction to the computation are shown in figure 7. A comparison of figure 6 with 7 shows an improvement in the prediction of yaw acceleration and a slight degradation in the prediction of pitch acceleration with little change in the prediction of roll acceleration. A further improvement in the predicted angular accelerations probably could be made with an inclusion of the effect of the drag force vectors on the moments; however, the values of pitch and yaw acceleration are small, and the addition probably would not appreciably affect the major upset about the roll axis.

DISCUSSION

A measure of the adequacy of the mathematical model used in the present studies to predict upset responses is shown in figure 8, where the predicted peak roll acceleration $\dot{p}_{V_{pred}}$ is plotted against the measured peak roll acceleration $\dot{p}_{V_{meas}}$. The circular symbols show the results in which the wake is adequately represented by a single pair of vortices. The square symbols show the results for cases in which the two-vortex model is inadequate to describe the wake. The flagged symbols indicate flights in which the spoilers on the 747 were deployed; the overprediction of peak roll acceleration is much greater for these cases and is discussed below. The quality of velocity fit, however, does not appear to be configuration dependent. The dashed lines form boundaries of ±30% of perfect correlation as shown by the solid line. For the most part, the values of $\dot{p}_{V_{pred}}$ are within these boundaries if the wake model provides a good fit to the velocity profile.

An anomalous case is the one in which the peak roll acceleration was measured at 1.6 rad/sec^2 and predicted to be 6.2 rad/sec^2 as shown in figure 9. The fit to the velocity measurements is shown in figure 10 to be reasonable, particularly in the proximity of the first vortex encountered. This large overprediction and the short time (about 0.1 sec) from zero to maximum angular acceleration suggested that aerodynamic lag might be important. Accordingly, the rate of increase of lift on an airfoil entering an arbitrary gust was calculated as suggested in references 35 and 36 and incorporated into the strip theory. A comparison of the predicted roll accelerations with and without the aerodynamic lag is shown in figure 11. It is concluded from this result that aerodynamic lag effects are not important during wake vortex encounters. It should be noted that for encounters of primary interest, where the penetrating

aircraft enters the wake at a small intercept angle thereby increasing the duration, the aerodynamic lag effects should be even less important. The aerodynamic lag effects, therefore, were not included in the mathematical upset response model developed in Appendix A.

There are two cases in figure 8 that show peculiar characteristics in which no discernible roll acceleration was measured in the vicinity of the left vortex, but a peak value of nearly 2 rad/sec^2 was predicted. Time histories of the angular accelerations from one case are shown in figure 12. It is seen that a definite disturbance about all three axes is predicted near 0.9 sec whereas none was measured. The velocity profiles for this case are shown in figure 13. The measured velocities are not well defined by the velocity profile model. The vertical-velocity gradient at about 0.9 sec indicates the presence of a vortex. The absence of a peak in the lateral velocity at this time means the probe must have passed through the core. The mathematical model thus places this vortex very near the flight path. Because the model requires the strength of both vortices to be equal, this results in an overestimation of vertical-velocity gradient for the left vortex and an underestimation for the right vortex. This is reflected in the angular accelerations (fig. 12) when a rolling acceleration is predicted where none exists for the left vortex, and the magnitude of the acceleration resulting from the right vortex is underpredicted. Measured angular acceleration-time histories very similar to the measurements shown in figure 12 are shown in figure 14, where the peak roll acceleration was predicted to be negligible in the vicinity of the left vortex. The velocity profiles for this case are well represented by the mathematical model as shown in figure 15.

In general, if the characteristics of the wake are well represented by the vortex model, the maximum roll acceleration can be predicted within 30%. If the vortices dissipate unevenly or more than one vortex pair exists in the wake, the vortex model used in this study does not adequately represent the wake and the vortex encounter may not be as severe as predicted.

CONCLUDING REMARKS

A flight test investigation has been conducted to develop a method for the prediction of upset responses of an aircraft from a known wake-vortex encounter. The results of this investigation can be summarized as follows.

1. The vortex-induced angular accelerations can be predicted within 30% if the characteristics of the wake are well represented by the vortex model.

2. The vortex model used in the present study adequately represents the wake if the vortices dissipate symmetrically and only one vortex pair exists in the wake.

3. The adequacy of the vortex model to describe the wake flow characteristics is not dependent on the configuration of the generating aircraft.

4. Aerodynamic lag effects are not important during wake vortex encounters.

APPENDIX A

PROCEDURES FOR PREDICTION OF VORTEX-INDUCED ANGULAR ACCELERATIONS

Equations for the calculation of the vortex-induced angular accelerations as used in simulation studies are shown below.

$$\dot{p}_v = \frac{\bar{q}}{I_x}\left[-\sum_{i=1}^{20}\left(C_{L_{\alpha_i}}\alpha_i S_i y_i\right)_{RW,LW} - \sum_{i=1}^{6}\left(C_{L_{\alpha_H}}\alpha_i S_i y_i\right)_{RHT,LHT} + \sum_{i=1}^{6}\left(C_{Y_{\beta_T}}\beta_i S_i z_i\right)_{VT}\right]$$

$$\dot{q}_v = \frac{\bar{q}}{I_y}\left[\sum_{i=1}^{20}\left(C_{L_{\alpha_i}}\alpha_i S_i x_i\right)_{RW,LW} + \sum_{i=1}^{6}\left(C_{L_{\alpha_H}}\alpha_i S_i x_i\right)_{RHT,LHT} + M_{\alpha_F}\alpha_F\right]$$

$$\dot{r}_v = \frac{\bar{q}}{I_z}\left[-\sum_{i=1}^{6}\left(C_{Y_{\beta_T}}\beta_i S_i x_i\right)_{VT} + N_{\beta_F}\beta_F\right]$$

The force vectors are calculated with respect to a local wind-axes system at each strip; however, the chordwise components are ignored in the transformation to body axes. As a result, the contribution to pitch and yaw of the asymmetrically varying chordwise component is neglected.

For the present tests, the contribution of the horizontal tail was omitted, and the forces and moments were calculated in the body-axes system, as follows

$$\dot{p}_v = \frac{\bar{q}}{I_x}\left\{-\sum_{i=1}^{20}\left[C_{L_{\alpha_i}}(\alpha_i + \alpha_{IC})S_i y_i \cos(\alpha_i + \alpha_{IC})\right]_{RW,LW} + \sum_{i=1}^{6}\left[C_{Y_{\beta_T}}(\beta_i + \beta_{IC})S_i z_i \cos(\beta_i + \beta_{IC}) - C_{Y_{\beta_T}}\beta_{IC}S_i z_i \cos\beta_{IC}\right]_{VT}\right\}$$

$$\dot{q}_v = \frac{\bar{q}}{I_y}\left\{\sum_{i=1}^{20}\left[C_{L_{\alpha_i}}(\alpha_i + \alpha_{IC})S_i x_i \cos(\alpha_i + \alpha_{IC}) - C_{L_{\alpha_i}}\alpha_{IC}S_i x_i \cos\alpha_{IC}\right]_{RW,LW}\right.$$

$$+\sum_{i=1}^{20}\left[C_{L_{\alpha_i}}(\alpha_i + \alpha_{IC})S_i z_i \sin(\alpha_i + \alpha_{IC}) - C_{L_{\alpha_i}}\alpha_{IC}S_i z_i \sin\alpha_{IC}\right]_{RW,LW}$$

$$+\sum_{i=1}^{6}\left[C_{Y_{\beta_T}}(\beta_i + \beta_{IC})S_i z_i \sin(\beta_i + \beta_{IC}) - C_{Y_{\beta_T}}\beta_{IC}S_i z_i \sin\beta_{IC}\right]_{VT}\cos\alpha_{IC}$$

$$-\sum_{i=1}^{6}\left[C_{Y_{\beta_T}}(\beta_i + \beta_{IC})S_i x_i \sin(\beta_i + \beta_{IC}) - C_{Y_{\beta_T}}\beta_{IC}S_i x_i \sin\beta_{IC}\right]_{VT}\sin\alpha_{IC}$$

$$\left. + M_{\alpha_F}\alpha_F\right\}$$

$$\dot{r}_v = \frac{\bar{q}}{I_z}\left\{-\sum_{i=1}^{20}\left[C_{L_{\alpha_i}}(\alpha_i + \alpha_{IC})S_i y_i \sin(\alpha_i + \alpha_{IC})\right]_{RW,LW}\right.$$

$$-\sum_{i=1}^{6}\left[C_{Y_{\beta_T}}(\beta_i + \beta_{IC})S_i x_i \cos(\beta_i + \beta_{IC}) - C_{Y_{\beta_T}}\beta_{IC}S_i x_i \cos\beta_{IC}\right]_{VT}$$

$$\left. + N_{\beta_F}\beta_F\right\}$$

where x_i, y_i, z_i are body-axes coordinates of the intersection of the 0.25-chord line and the centerline of each strip.

The coordinates x_i, y_i, z_i and the areas S_i of the strips were calculated with the use of strip theory geometry. For example,

$$x_i = x_o - \left(i - \frac{1}{2}\right)\Delta x$$

and similarly for y_i, z_i, and S_i. For the present tests, the wing was divided into 20 strips per semispan and the vertical tail into 6 strips. Initial values and increments used for the wing and vertical tail are listed in table 2.

The incremental angles of attack α_i and sideslip β_i resulting from the vortex flow field were calculated for use in the strip theory as follows. With the location $h_{1,2}$ and $d_{1,2}$ of the vortex pair from an arbitrary initial point on the flight path as determined from the velocity profile measurements, the vortex-axes system was set such that the origin was midway between the two vortices with their centers on the lateral axis. The coordinates of the origin and the orientation of the vortex axes were computed as

$$y_{v_o} = \frac{h_1 + h_2}{2}$$

$$z_{v_o} = \frac{d_1 + d_2}{2}$$

$$\tan \mu = \frac{d_2 - d_1}{h_2 - h_1}$$

with the distance between the two vortices being

$$2d = \sqrt{(h_2 - h_1)^2 + (d_2 - d_1)^2}$$

The center-of-gravity location of the probe aircraft was transformed from Earth axes to the vortex axes.

$$\begin{bmatrix} y_{cg} \\ z_{cg} \end{bmatrix}_v = \begin{bmatrix} \cos \mu & \sin \mu \\ -\sin \mu & \cos \mu \end{bmatrix} \left\{ \begin{bmatrix} y \\ z \end{bmatrix}_{cg} - \begin{bmatrix} y_v \\ z_v \end{bmatrix}_o \right\}$$

Then the point of interest on a strip was transformed from the body axes to the vortex axes.

$$\begin{bmatrix} y \\ z \end{bmatrix}_v = \begin{bmatrix} y_{cg} \\ z_{cg} \end{bmatrix}_v + \begin{bmatrix} T \end{bmatrix} \begin{bmatrix} x \\ y \\ z \end{bmatrix}_i$$

where

$$[T] = \begin{bmatrix} \sin\psi\cos\theta\cos\mu - \sin\theta\sin\mu & \sin\psi\sin\theta\sin\phi\cos\mu - \cos\psi\cos\phi\cos\mu + \cos\theta\sin\phi\sin\mu & \sin\psi\sin\theta\cos\phi\cos\mu - \cos\psi\sin\phi\cos\mu + \cos\theta\cos\phi\sin\mu \\ -\sin\psi\cos\theta\cos\mu - \sin\theta\cos\mu & -\sin\psi\sin\theta\sin\phi\sin\mu + \cos\psi\cos\phi\sin\mu + \cos\theta\sin\phi\cos\mu & -\sin\psi\sin\theta\cos\phi\sin\mu + \cos\psi\sin\phi\sin\mu + \cos\theta\cos\phi\cos\mu \end{bmatrix}$$

The local velocity components due to the left and right vortices were computed in the vortex-axes system.

$$v_v = -\frac{\Gamma}{2\pi}\left[\frac{z_v}{r_1^2}\left(1 - e^{-\beta_v r_1^2}\right) - \frac{z_v}{r_2^2}\left(1 - e^{-\beta_v r_2^2}\right)\right]$$

$$w_v = \frac{\Gamma}{2\pi}\left[\frac{y_v + d}{r_1^2}\left(1 - e^{-\beta_v r_1^2}\right) - \frac{y_v - d}{r_2^2}\left(1 - e^{-\beta_v r_2^2}\right)\right]$$

where

$$r_{1,2} = \sqrt{z_v^2 + (y_v \pm d)^2}$$

These velocity components were transformed back to the body axes,

$$\begin{bmatrix} v \\ w \end{bmatrix}_i = [T]^{-1} \begin{bmatrix} 0 \\ v \\ w \end{bmatrix}_v$$

and the incremental angles of attack and sideslip were computed as

$$\alpha_i = -\frac{w_i}{V}$$

$$\beta_i = -\frac{v_i}{V}$$

The forces were applied at the 0.25-chord location, but the incremental force on each strip was assumed to be proportional to the incremental angle at the 0.75-chord location of the strip; therefore, the values of x_o and λ from table 2 were changed to the following values for the computation of α_i and β_i.

	Wing	Vertical tail
x_o	-0.9 m (-2.8784 ft)	-5.2 m (-17.1412 ft)
λ	5.73°	21.68°

Stall on each strip was represented by a limitation of the force vectors such that their magnitudes were approximately constant outside the limits of maximum and minimum angles of attack and sideslip.

$$(\alpha_{min} - \alpha_{dyn}) \leq (\alpha_i + \alpha_{IC}) \leq (\alpha_{max} - \alpha_{dyn})$$

$$(\beta_{min} - \beta_{dyn}) \leq (\beta_i + \beta_{IC}) \leq (\beta_{max} - \beta_{dyn})$$

where

$$\alpha_{dyn} = \frac{py_i - qx_i}{V}$$

$$\beta_{dyn} = \frac{rx_i - pz_i}{V} \quad .$$

These limitations on angles were applied only in determining the magnitudes of the force vectors and not in determining the direction of action of the vectors. The maximum and minimum angles of attack and sideslip are listed in table 3 along with other parameters used in the strip theory.

APPENDIX B

CORRECTIONS TO MEASURED ANGULAR ACCELERATIONS

To obtain the angular accelerations due to the vortex flow field, the measured values of acceleration must be corrected for the aerodynamic accelerations that the aircraft would have experienced in the absence of the vortex. The vortex-induced angular accelerations were obtained by subtracting the accelerations resulting from the aircraft attitude, control surface deflections, and angular rates from the total accelerations measured.

$$\dot{p}_v = \dot{p} - \frac{\bar{q}Sb}{I_x}\left[C_{\ell_\beta}\beta_c + C_{\ell_{\delta_a}}\delta_a + C_{\ell_{\delta_r}}\delta_r + \frac{b}{2V}\left(C_{\ell_p}p + C_{\ell_r}r\right)\right]$$

$$\dot{q}_v = \dot{q} - \frac{\bar{q}Sc}{I_y}\left(C_{m_o} + C_{m_\alpha}\alpha_c + C_{m_{\delta_e}}\delta_e + \frac{c}{2V}C_{m_q}q\right)$$

$$\dot{r}_v = \dot{r} - \frac{\bar{q}Sb}{I_z}\left[C_{n_\beta}\beta_c + C_{n_{\delta_a}}\delta_a + C_{n_{\delta_r}}\delta_r + \frac{b}{2V}\left(C_{n_p}p + C_{n_r}r\right)\right]$$

The effective angles of attack and sideslip α_c and β_c were determined from the normal and lateral accelerations measured at the center-of-gravity location.

$$\alpha_c = \frac{W a_n}{C_{N_\alpha}\bar{q}S}$$

$$\beta_c = -\frac{W a_y}{C_{Y_\beta}\bar{q}S} \quad .$$

The pitching-moment coefficient required to trim the aircraft C_{m_o} was determined by setting the pitching moment equal to zero prior to vortex encounter. The aerodynamic coefficients were determined from the results of flight and wind-tunnel tests (refs. 24, 37, and 38).

The aircraft characteristics and aerodynamic coefficients that were used in the present tests are listed in table 4.

REFERENCES

1. Israel, D. R.: Air Traffic Control: Upgrading the Third Generation. Technology Review, vol. 77, no. 3, January, 1975, pp. 14-24.

2. Brashears, M. R.; Hallock, J. N.; and Logan, N. A.: Analysis of Predicted Aircraft Wake Vortex Transport and Comparison with Experiment. AIAA Paper 74-506, 1974 (to be published in J. Aircraft).

3. Hallock, J. N.; and Goldstone, L.: US/UK Vortex Monitoring Program at Heathrow Airport. AGARD Guidance and Control Panel 20th Symposium on Plans and Developments for Air Traffic Systems, Paper 24, 1975.

4. Hallock, J. N.; Wood, W. D.; and Spitzer, E. A.: The Motion of Wake Vortices in the Terminal Environment. AIAA/AMS Sixth Conference on Aerospace and Aeronautical Meteorology, Preprint Volume, 1974, pp. 393-398.

5. Brashears, M. R.; and Hallock, J. N.: Aircraft Wake Vortex Transport Model. J. Aircraft, vol. 11, no. 5, 1974, pp. 265-272.

6. Brashears, M. R.; and Hallock, J. N.: A Predictive Model of Wake Vortex Transport. AIAA/AMS Sixth Conference on Aerospace and Aeronautical Meteorology, Preprint Volume, 1974, pp. 387-392.

7. Rossow, V. J.; Corsiglia, V. R.; Schwind, R. G.; Frick, J. K. D.; and Lemmer, O. J.: Velocity and Rolling Moment Measurements in the Wake of a Swept Wing Model in the 40- by 80-Foot Wind Tunnel. NASA TM X-62,414, 1975.

8. Corsiglia, V. R.; Jacobsen, R. A.; and Chigier, N.: An Experimental Investigation of Trailing Vortices Behind a Wing with a Vortex Dissipator. Aircraft Wake Turbulence and Its Detection; edited by J. Olsen, A. Goldberg, and M. Rogers. Pensum Press, New York, 1971.

9. Wentz, W. R., Jr.: Evaluation of Several Vortex Dissipators by Wind Tunnel Measurements of Vortex-Induced Upset Loads. Aeronautical Rept. 72-3, Wichita State Univ., Sept. 1972.

10. Banta, A. J.: Effects of Planform and Mass Injection on Rolling Moments Induced by Trailing Vortices. M. S. Thesis, Wichita State Univ., Dec. 1973.

11. Kirkman, K. L.; Brown, C. E.; and Goodman, A.: Evaluation of Effectiveness of Various Devices for Attenuation of Trailing Vortices Based on Model Test in a Large Towing Basin. NASA CR-2202, Dec. 1973.

12. Hastings, E. C., Jr.; Shanks, R. E.; Champine, R. A.; and Copeland, W. L.: Preliminary Results of Flight Tests of Vortex Attenuating Splines. NASA TM X-71928, 1974.

13. Corsiglia, V. R.; Rossow, V. J.; and Ciffone, D. L.: Experimental Study of the Effect of Span Loading on Aircraft Wakes. AIAA Paper 75-885, 1975 (see also NASA TM X-62,431, 1975).

14. Hastings, E. C., Jr.; Patterson, J. C., Jr.; Shanks, R. A.; Champine, R. A.; Copland, W. L.; and Young, D. C.: Development and Flight Test of Vortex Attenuating Splines. NASA TN D-8083, Sept. 1975.

15. Patterson, J. C., Jr.: Vortex Attenuation Obtained in the Langley Vortex Research Facility. J. Aircraft, vol. 12, no. 9, Sept. 1975. pp. 745-749.

16. Ciffone, Donald L.: Vortex Interactions in Multiple Vortex Wakes Behind Aircraft. AIAA Paper 76-62, 1976.

17. Bilanin, A. J.; and Widnall, S. E.: Aircraft Wake Dissipation by Sinusoidal Instability and Vortex Breakdown. AIAA Paper 73-107, 1973.

18. Jacobsen, R. A.; and Short, B. J.: A Flight Investigation of the Wake Turbulence Alleviation Resulting from a Flap Configuration Change on a B-747 Aircraft. NASA TM-73,263, 1977.

19. Johnson, W. A.; and Rediess, H. A.: Study of Control System Effectiveness in Alleviating Vortex Wake Upsets. AIAA Paper 73,833, 1973.

20. Jewell, W. F.; and Stapleford, R. L.: Mathematical Models Used to Simulate Aircraft Encounter with Wake Vortices. STI TR-1035-4, 1975.

21. Sammonds, R. I.; and Stinnett, G. W., Jr.: Hazard Criteria for Wake Vortex Encounters. NASA TM X-62,473, 1975.

22. Sammonds, R. I.; Stinnett, G. W., Jr.; and Larsen, W. E.: Wake Vortex Encounter Hazard Criteria for Two Aircraft Classes. NASA TM X-73,113 1976 (FAA RD-75-206, 1976).

23. Sammonds, R. I.; Stinnett, G. W., Jr.; and Larsen, W. E.: Criteria Relating Wake Vortex Encounter Hazard to Aircraft Response. J. Aircraft, vol. 14, no. 10, 1977, pp. 981-989.

24. Robinson, G. H.; and Larson, R. R.: A Flight Evaluation of Methods for Predicting Vortex Wake Effects on Trailing Aircraft. NASA TN D-6904, 1972.

25. Croom, Delwin R.: Low-Speed Wind-Tunnel Investigation of Forward-Located Spoilers and Trailing Splines as Trailing Vortex Hazard Alleviation Devices on an Aspect-Ratio-8 Wing Model. NASA TM X-3166, 1975.

26. Croom, Delwin R.; and Dunham, R. Earl, Jr.: Low-Speed Wind-Tunnel Investigation of Span Load Alteration, Forward-Located Spoilers, and Splines as Trailing-Vortex Hazard Alleviation Devices on a Transport Aircraft Model. NASA TN D-8133, 1975.

27. Croom, Delwin R.: Low-Speed Wind-Tunnel Investigation of Various Segments of Flight Spoilers as Trailing-Vortex-Alleviation Devices on a Transport Aircraft Model. NASA TN D-8162, 1976.

28. Barber, Marvin R.; Hastings, Earl C., Jr.; Champine, Robert A.; and Tymczyszyn, Jospeh J.: Vortex Attenuation Flight Experiments. NASA SP-409, 1977.

29. Lamb, Sir Horace: Hydrodynamics, Sixth Edition. Dover Publications, Inc., New York, 1945.

30 Spreiter, J. R.; and Sacks, A. H.: The Rolling-Up of the Trailing Vortex Sheet and Its Effect on the Downwash Behind Wings. J. Aeronaut. Sci., vol. 18, no. 1, Jan. 1951, pp. 21-32.

31. Bilanin, A. J.; and Donaldson, C. du P.: Estimation of Velocities and Roll-Up in Aircraft Vortex Wakes. J. Aircraft, vol. 12, no. 7, July 1975, pp. 578-585.

32. Nelson, R. C.: The Response of Aircraft Encountering Aircraft Wake Turbulence. AFFDL TR 74-29, June 1974.

33. Nelson, R. C.; and McCormick, B. W.: The Dynamic Behavior of an Aircraft Encountering Aircraft Wake Turbulence. AIAA Paper 74-774, Aug. 1974.

34. Rossow, V. J.: Inviscid Modeling of Aircraft Trailing Vortices, Wake Vortex Minimization. NASA SP-409, 1976, pp. 9-59.

35. von Karman, Th.; and Sears, W. R.: Airfoil Theory for Non-Uniform Motion. Jour. Aero. Sci., vol. 5, no. 10, Aug. 1938, pp. 379-390.

36. Jones, Robert T.: The Unsteady Lift of a Wing of Finite Aspect Ratio. NACA Report 681, 1940.

37. Soderman, P. T.; and Aiken, T. N.: Full-Scale Wind-Tunnel Tests of a Small Unpowered Jet Aircraft with a T-Tail. NASA TND-6573, 1971.

38. Kurkowski, R. L.; Barber, M. R.; and Garodz, L. J.: Characteristics of Wake Vortex Generated by a Boeing 727 Jet Transport During Two-Segment and Normal Approach Flight Paths. NASA TN D-8222, 1976.

TABLE 1.- AIRCRAFT PHYSICAL CHARACTERISTICS

(a) B-747, wake generator aircraft

Length, m (ft)	70.51	(231.33)
Height, m (ft)	19.33	(63.42)
Wing:		
Area, m^2 (ft^2)	511	(5,500)
Span, m (ft)	59.64	(195.67)
Aspect ratio	6.96	
Sweep at quarter chord, deg	37.5	
Mean aerodynamic chord, m (ft)	8.33	(27.32)
Incidence angle, deg	2	
Dihedral angle, deg	7	
Taper ratio	.356	
Control surfaces:		
Rudder area, m^2 (ft^2)	22.9	(247)
Rudder deflection, deg	15	
Elevator area, m^2 (ft^2)	32.5	(350)
Elevator deflection, deg	-23 to 17	
Aileron area (total), m^2 (ft^2)	20.9	(222)
Aileron deflection, deg		
Inboard	20	
Outboard	-25 to 15	
Spoiler area (total), m^2 (ft^2)	30.8	(331)
Spoiler deflection, deg		
Panels 6 to 8	20	
Panels 1 to 4, 9 to 12	45	
Trailing-edge flap area (total), m^2 (ft^2)	78.7	(847)
Trailing-edge flap deflection, deg	30	
Leading-edge flap area (total), m^2 (ft^2)	48.1	(518)
Weight, kg (lb):		
Empty	158,220	(348,816)
Maximum takeoff	322,050	(710,000)

TABLE 1.- Concluded.

(b) Learjet 23 wake probe aircraft

Length, m (ft)	13.18	(43.25)
Height, m (ft)	3.83	(12.58)
Wing:		
Area, m^2 (ft^2)	21.6	(232.0)
Span, m (ft)	10.4	(34.10)
Aspect ratio	5.46	
Sweep at 25 percent chord, deg	13.0	
Mean aerodynamic chord, m (ft)	2.1	(7.04)
Control surfaces:		
Rudder area, m^2 (ft^2)	.67	(7.18)
Rudder deflection, deg	30.0	
Elevator area, m^2 (ft^2)	1.31	(4.13)
Elevator deflection, deg	14.0	
Aileron area, m^2 (ft^2)	1.08	(11.70)
Aileron deflection, deg	20.0	
Wing flap area, m^2 (ft^2)	3.42	(36.85)
Wing flap deflection, deg	40.0	
Weight, kg (lb):		
Empty	3300	(7275)
Takeoff	6124	(13,500)
Moments of inertia, kg-m^2 (slug-ft^2):		
Roll (empty)	8634	(6364)
Roll (full)	35,112	(25,880)
Pitch (empty)	22,258	(16,405)
Pitch (full)	26,765	(19,728)
Yaw (empty)	28,704	(21,157)
Yaw (full)	66,586	(49,079)

TABLE 2.- STRIP THEORY GEOMETRY VALUES

	Wing	Vertical tail
x_o	0.50 m (1.6316 ft)	-3.5 m (-11.544 ft)
Δx	$\Delta y \tan \lambda$	$\Delta z \tan \lambda$
y_o	0	0
Δy	$\frac{1}{20}\left(\frac{b}{2}\right)$	0
z_o	.34 m (1.12 ft)	-.09 m (-.29 ft)
Δz	0	$\frac{1}{6}$ (b)
S_o	$c_R \Delta y$	$c_R \Delta z$
ΔS	$\frac{1}{20}(c_R - c_T)\Delta y$	$\frac{1}{6}(c_R - c_T)\Delta z$
λ	13°	39.5°
b	10 m (34.10 ft)	2.4 m (7.83 ft)
c_R	2.7 m (9.02 ft)	3.4 m (11.193 ft)
c_T	1.4 m (4.57 ft)	1.4 m (4.51 ft)

TABLE 3.- NUMERICAL VALUES USED IN STRIP THEORY

Parameter	Wing	Vertical tail	Fuselage
α_{max}	12°	---	30°
α_{min}	-12°	---	-30°
β_{max}	---	20°	30°
β_{min}	---	-20°	-30°
$C_{L_{\alpha_i}}$	See below	---	---
$C_{y_{\beta_T}}$	---	1.6202	---
M_{α_F}	---	---	1.7 m^3/rad (59.406 ft^3/rad)
N_{β_F}	---	---	-12 m^3/rad (-424.96 ft^3/rad)

Strip, i	$C_{L_{\alpha_i}}$
1	6.672
2	6.672
3	6.672
4	5.719
5	4.766
6	4.647
7	4.528
8	4.409
9	4.289
10	4.170
11	4.051
12	3.932
13	3.813
14	3.694
15	3.575
16	3.455
17	3.336
18	2.383
19	1.430
20	0.477

TABLE 4.- AIRCRAFT CHARACTERISTICS AND AERODYNAMIC COEFFICIENTS ABOUT THE BODY AXES OF THE LEARJET WITH FLAPS AT 20°

Aerodynamics		
Coefficient	Value at $\alpha = 0$	Slope with α
C_{ℓ_β}	-0.103	-0.273
$C_{\ell_{\delta_a}}$	.0655	0
$C_{\ell_{\delta_r}}$	.0235	0
C_{ℓ_p}	-.410	0
C_{ℓ_r}	.194	1.56
C_{m_α}	-1.09	0
$C_{m_{\delta_e}}$	-1.29	0
C_{m_q}	-12.0	0
C_{n_β}	.115	-.141
$C_{n_{\delta_a}}$	-.006	0
$C_{n_{\delta_r}}$	-.0745	0
C_{n_p}	-.0365	-1.01
C_{n_r}	-.240	0
C_{N_α}	5.21	0
C_{Y_β}	-.665	0

Characteristics	
Parameter	Value
b	10.4 m (34.10 ft)
c	2.1 m (7.04 ft)
S	21.6 m^2 (232.ft^2)
W	51,155 N (11,500 lb)
I_x	25,252 kg-m^2 (18,625 slug-ft^2)
I_y	25,049 kg-m^2 (18,475 slug-ft^2)
I_z	52,430 kg-m^2 (38,670 slug-ft^2)

Figure 1.- Boeing 747 wake generator aircraft (center) and Learjet probe aircraft (top).

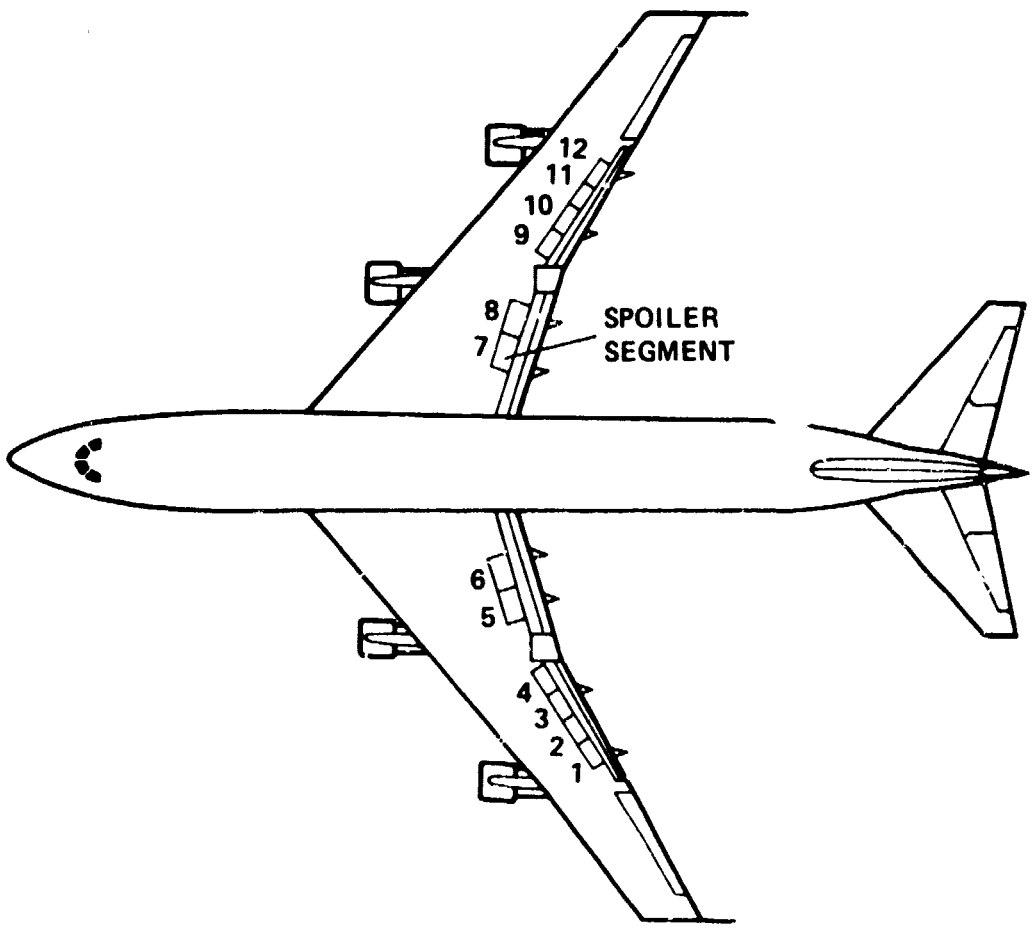

Figure 2.- Spoilers on B-747 airplane.

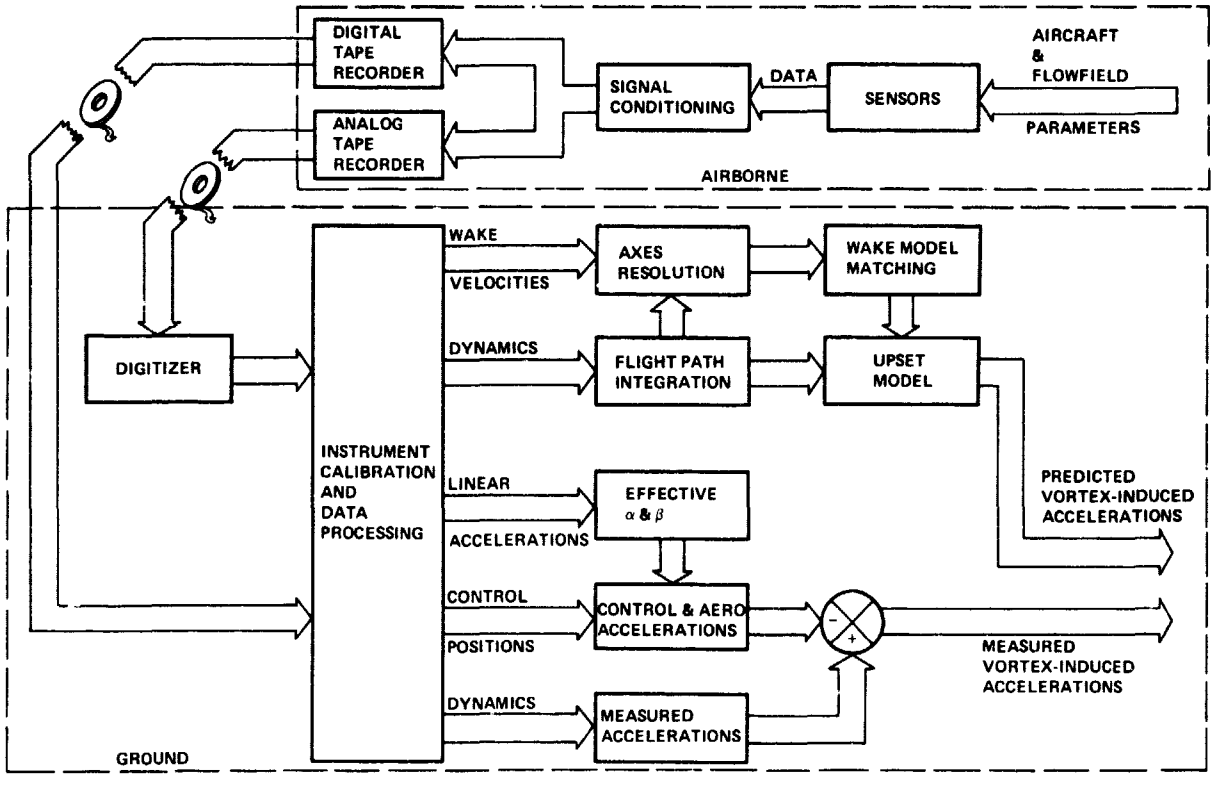

Figure 3.- Signal flow block diagram.

ORIGINAL PAGE IS
OF POOR QUALITY

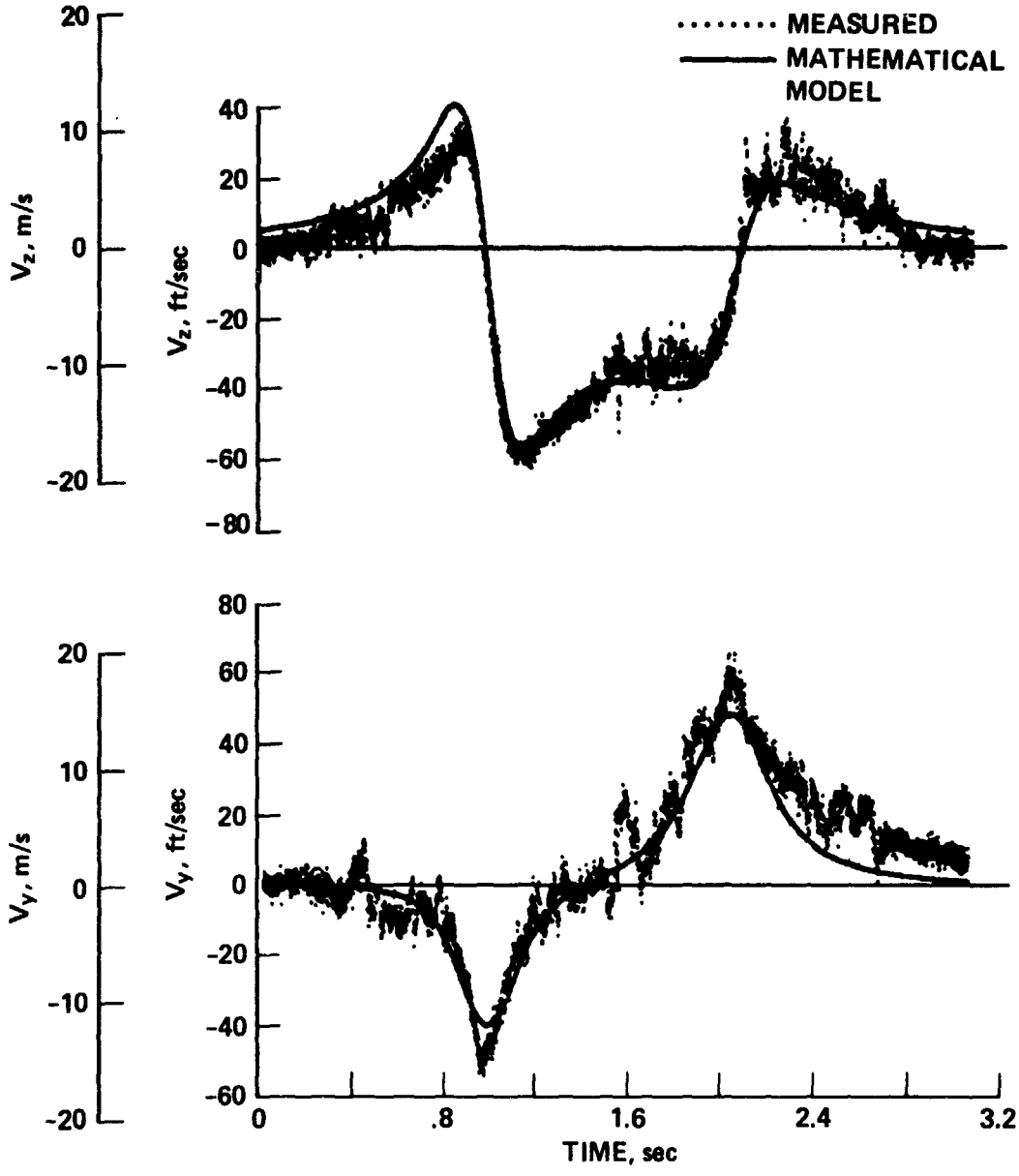

Figure 4.- Example of an adequate representation of vortex velocities by mathematical model. Separation distance 1.7 n. mi., spoilers not deployed.

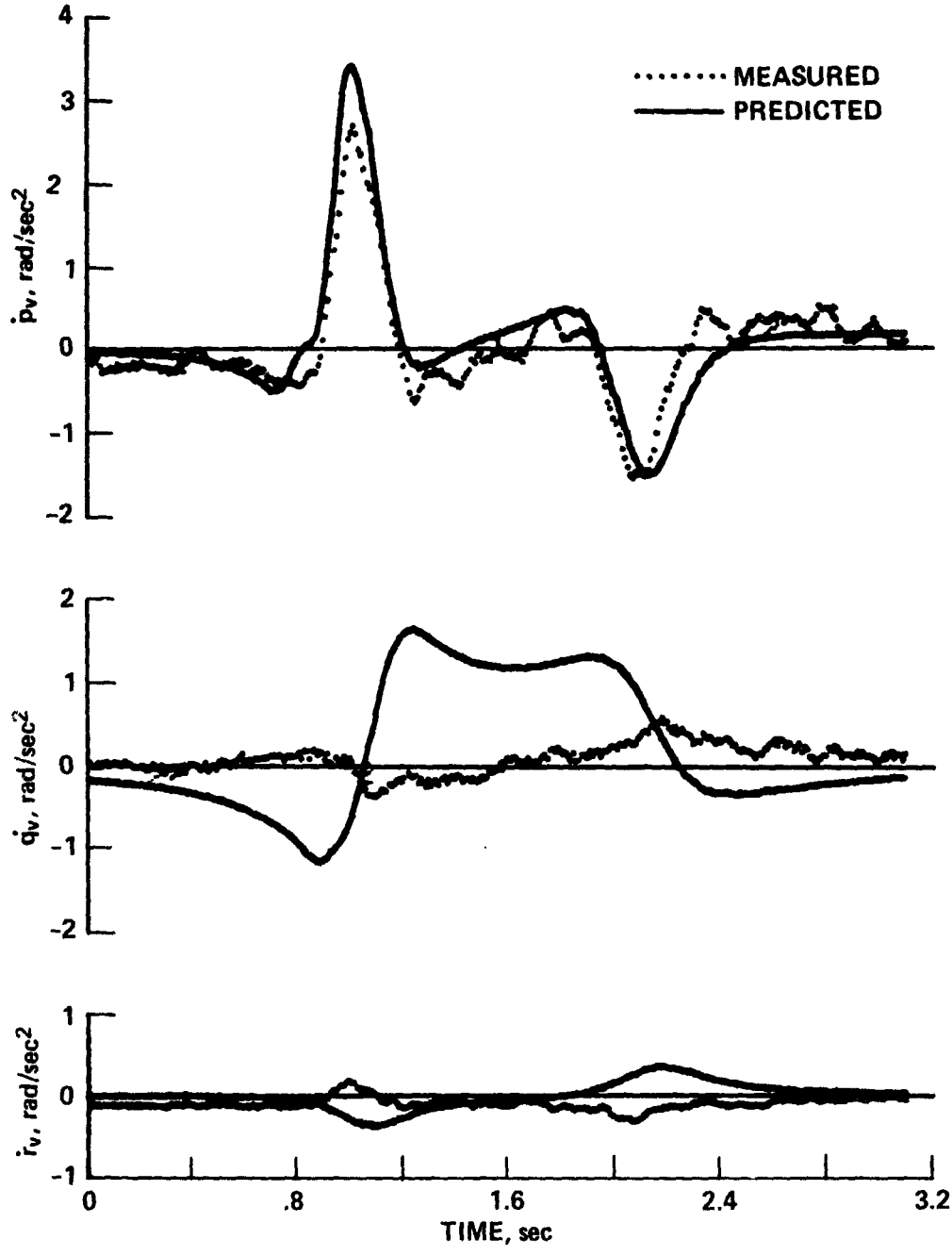

Figure 5.- Comparison of measured angular accelerations with values predicted by the mathematical model used in simulation studies.

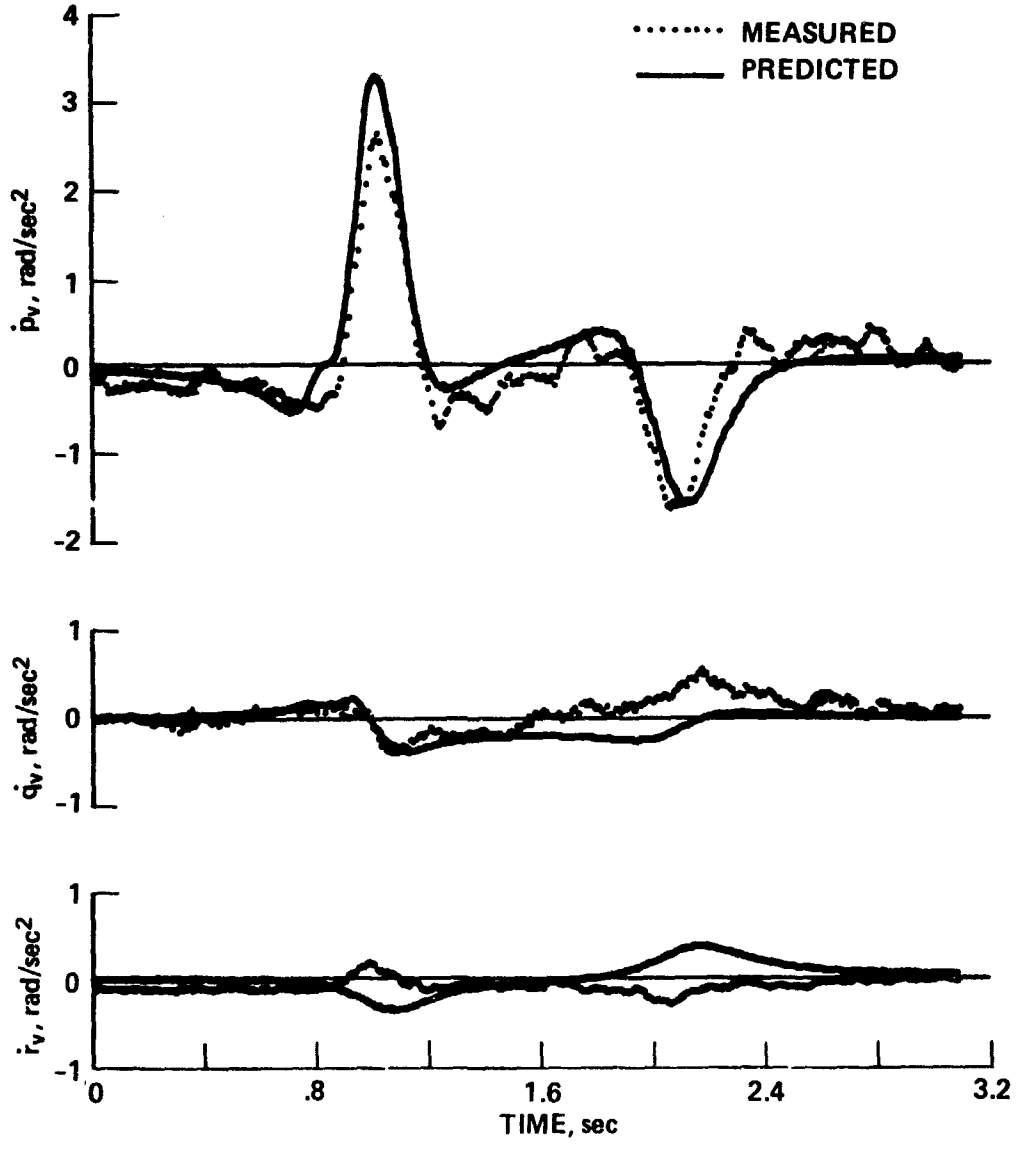

Figure 6.- Comparison of measured accelerations with values predicted by the improved mathematical model in which the vortex-induced horizontal-tail loads are zero.

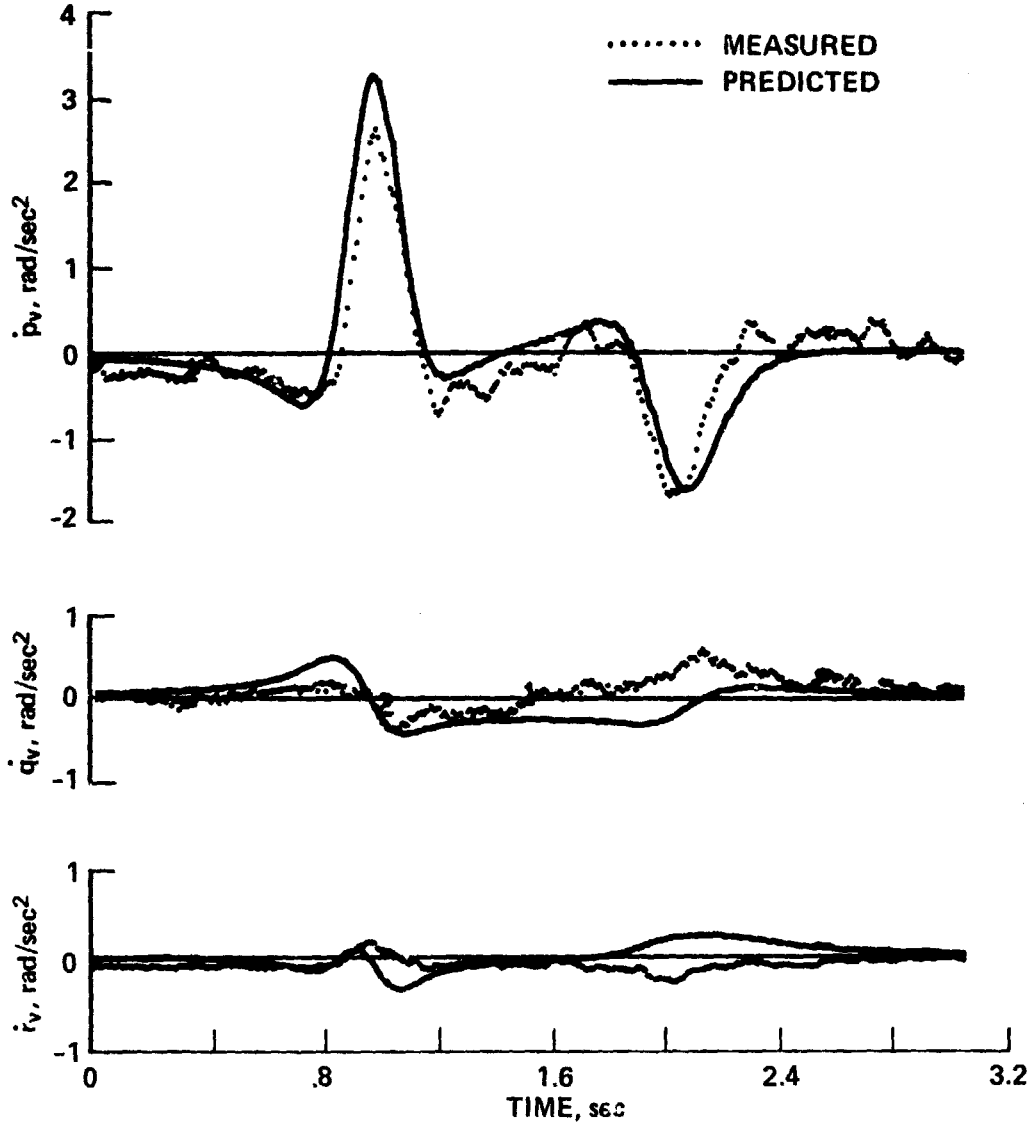

Figure 7.- Comparison of measured angular accelerations with values predicted by the corrected mathematical model that includes chordwise components of forces.

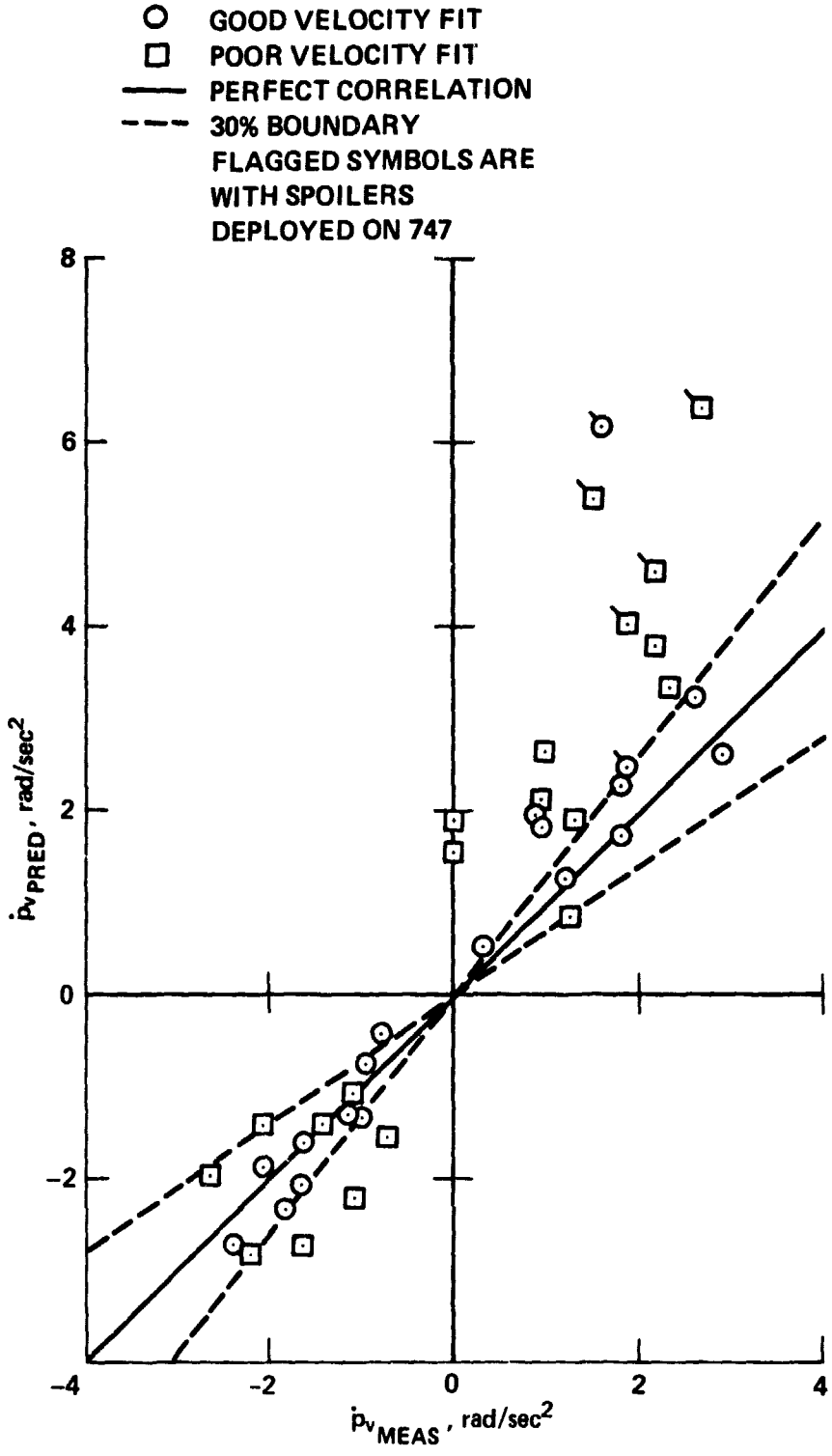

Figure 8.- Correlation of predicted values with measured values of peak roll acceleration.

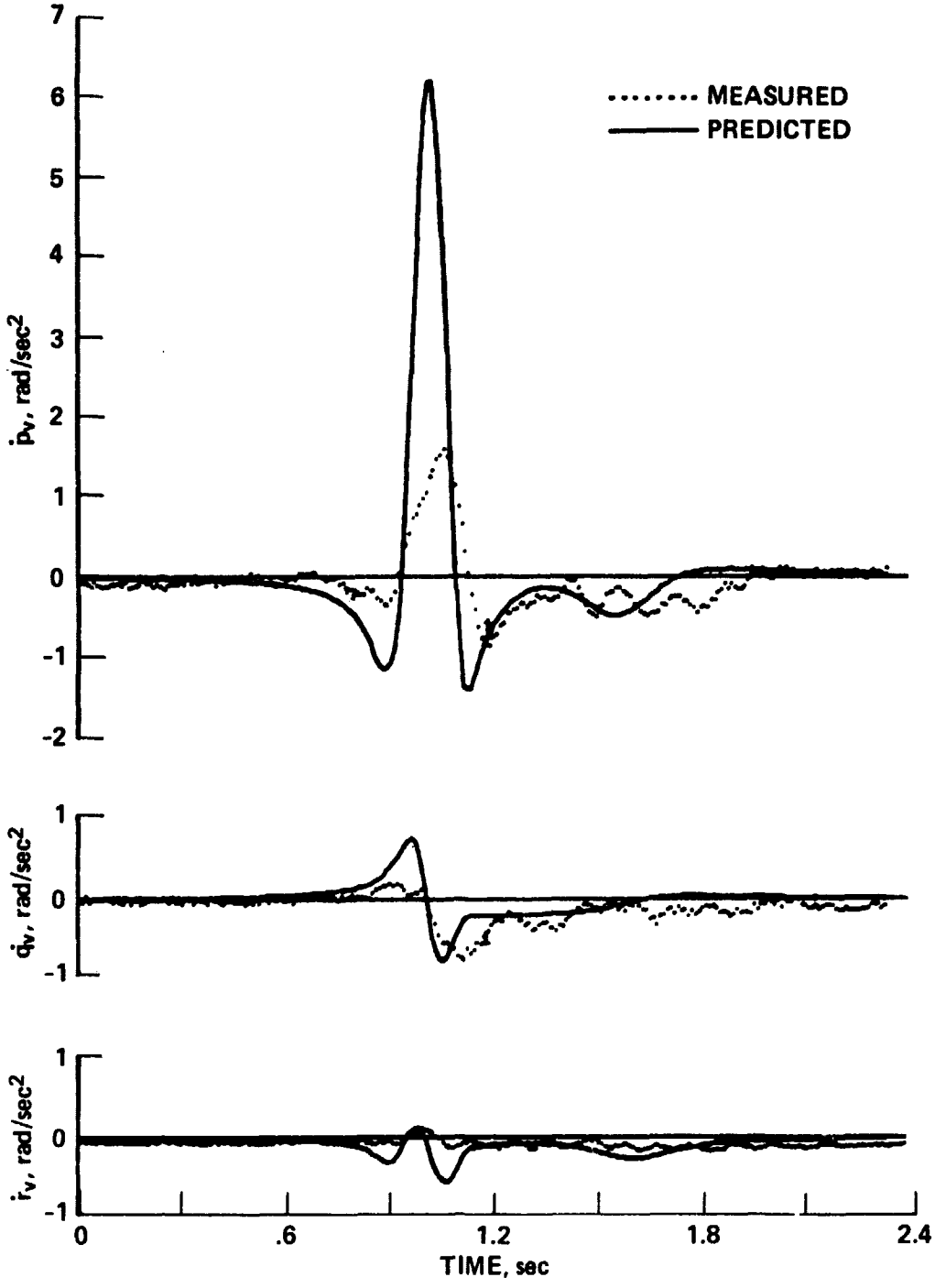

Figure 9.- Anomalous results of poor prediction of accelerations despite a good match of vortex model to velocity measurements.

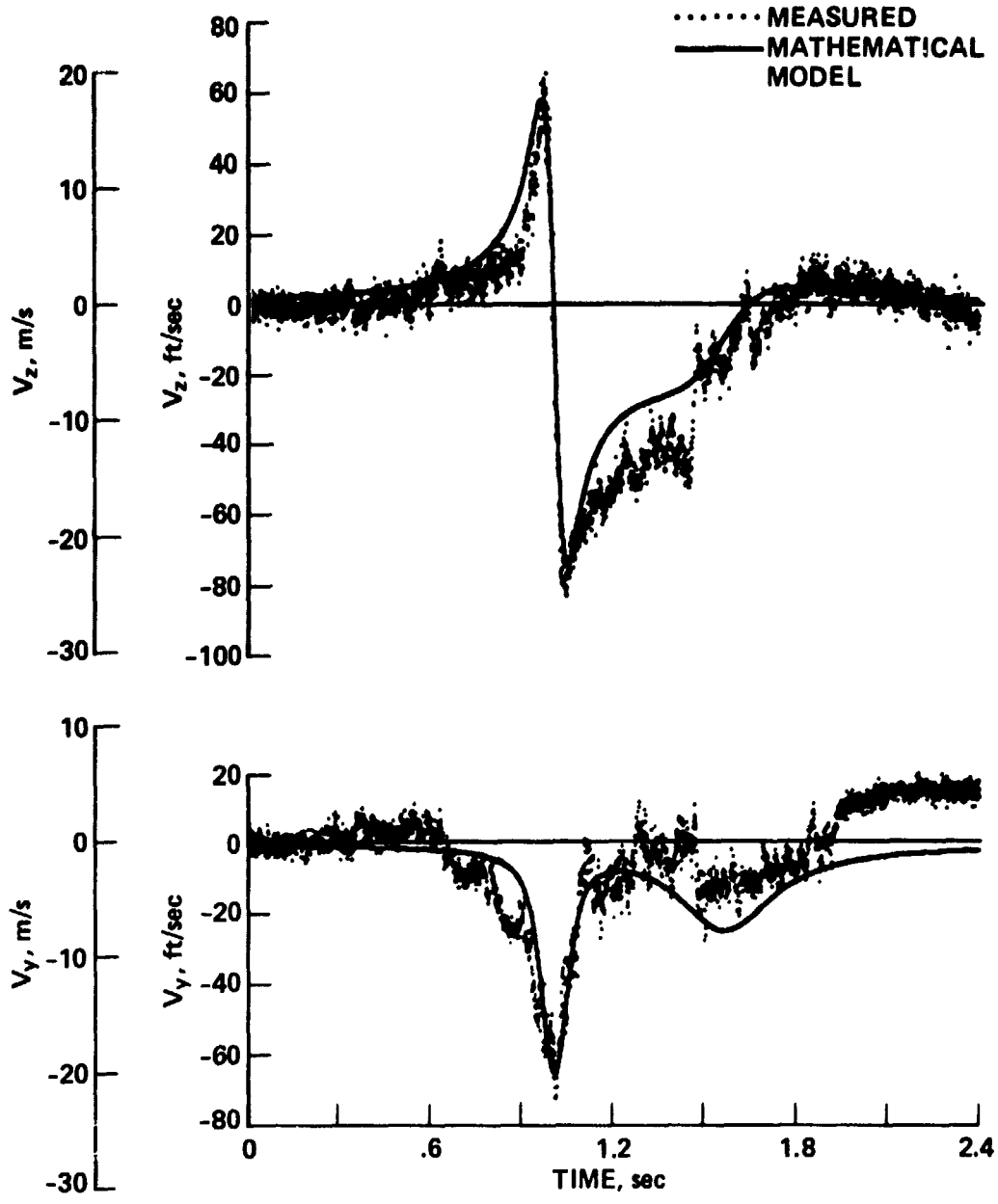

Figure 10.- Velocity profiles for results shown in figure 9.

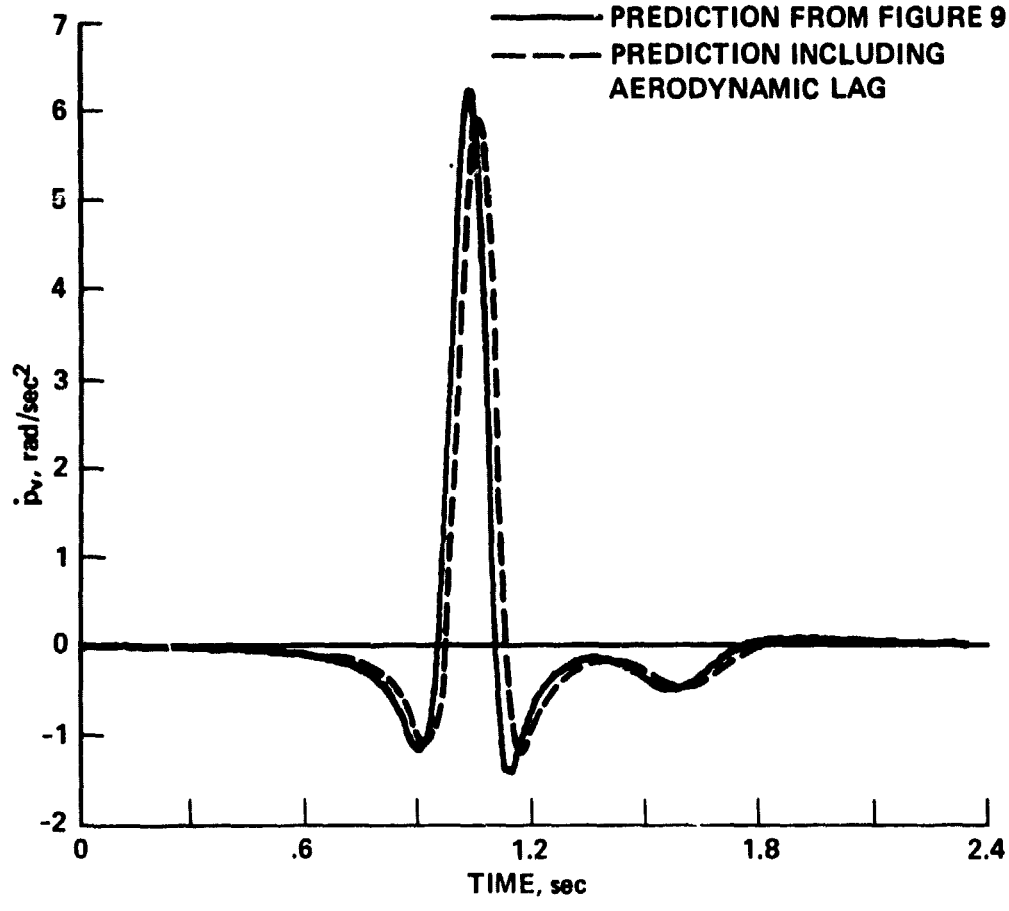

Figure 11.- Effect of aerodynamic lag on prediction of roll acceleration.

ORIGINAL PAGE IS
OF POOR QUALITY

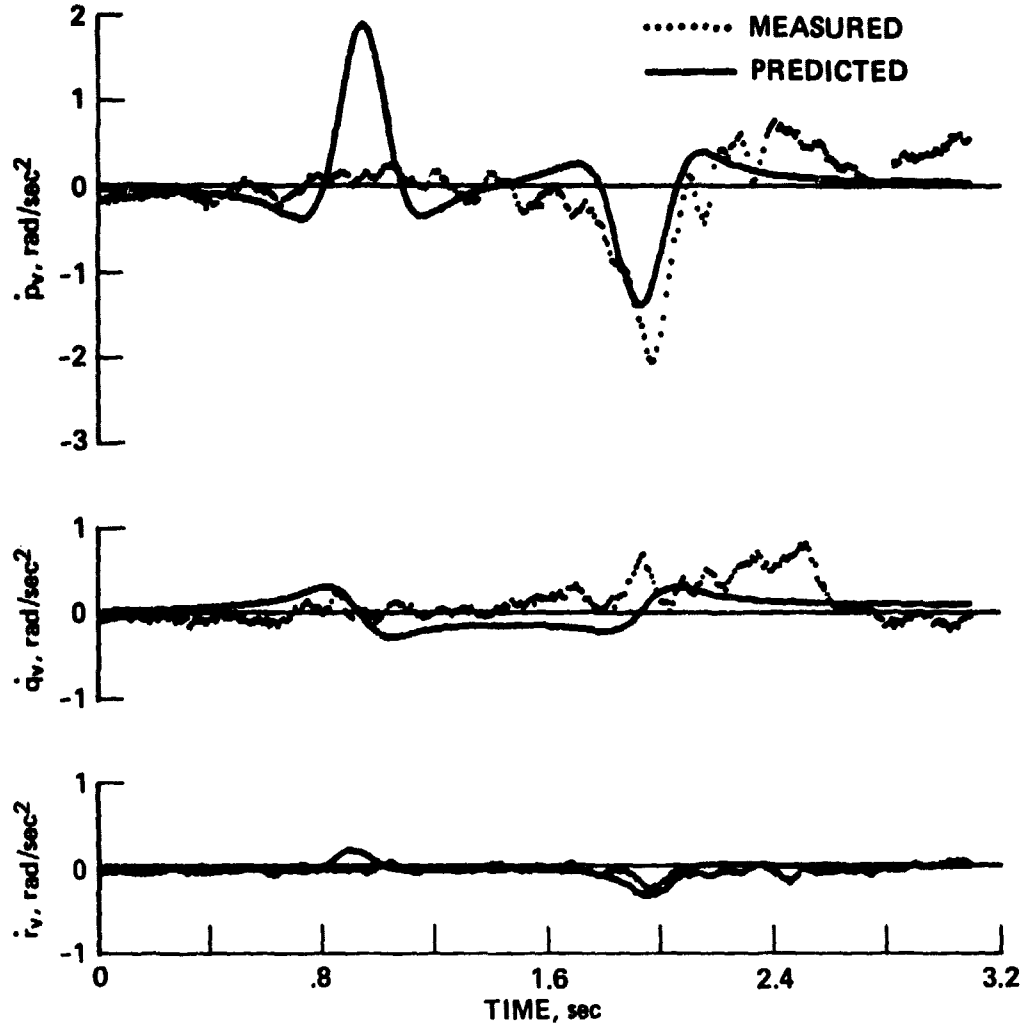

Figure 12.- Example of poor prediction of accelerations because of poor match of vortex model to velocity measurements.

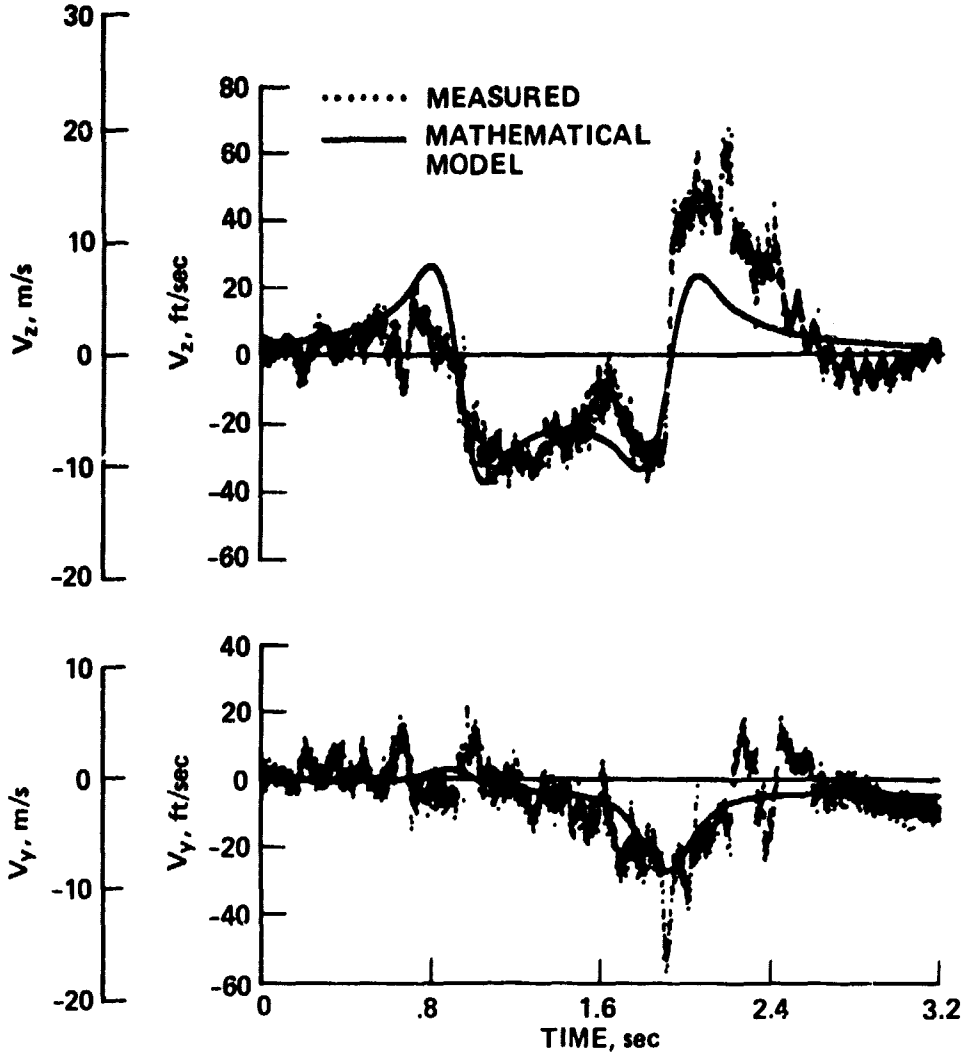

Figure 13.- Velocity profiles for results shown in figure 12.

ORIGINAL PAGE IS
OF POOR QUALITY

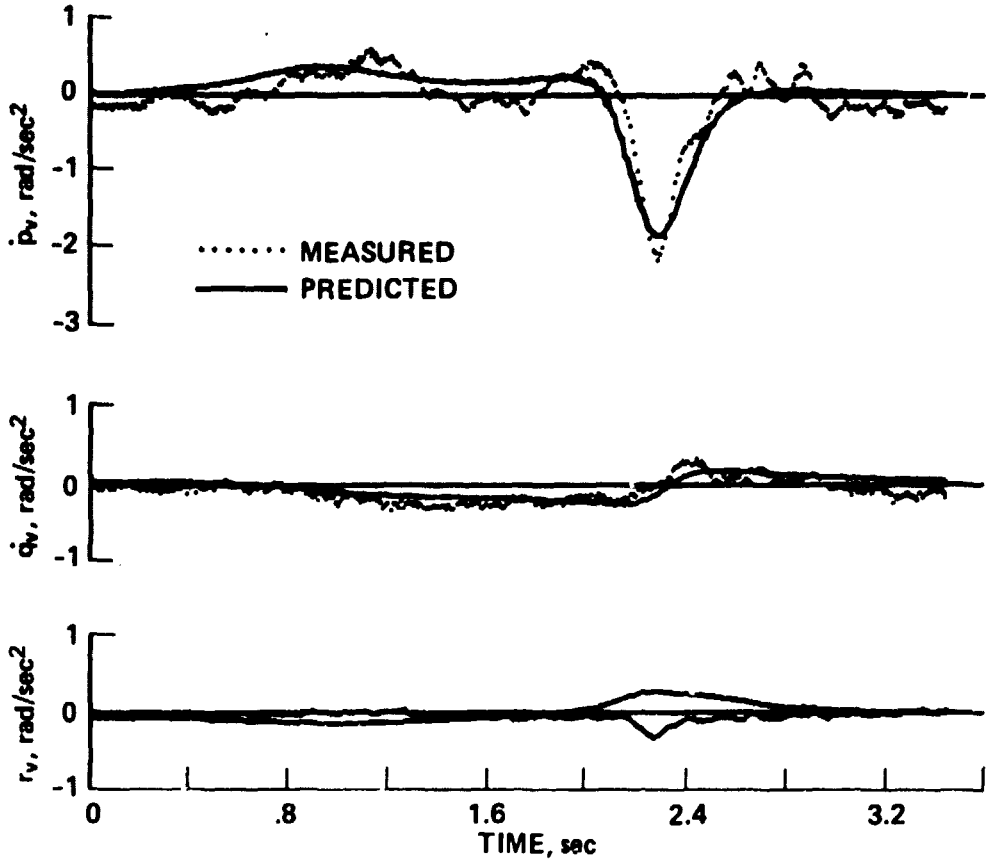

Figure 14.- Example of good match of predicted and measured angular accelerations.

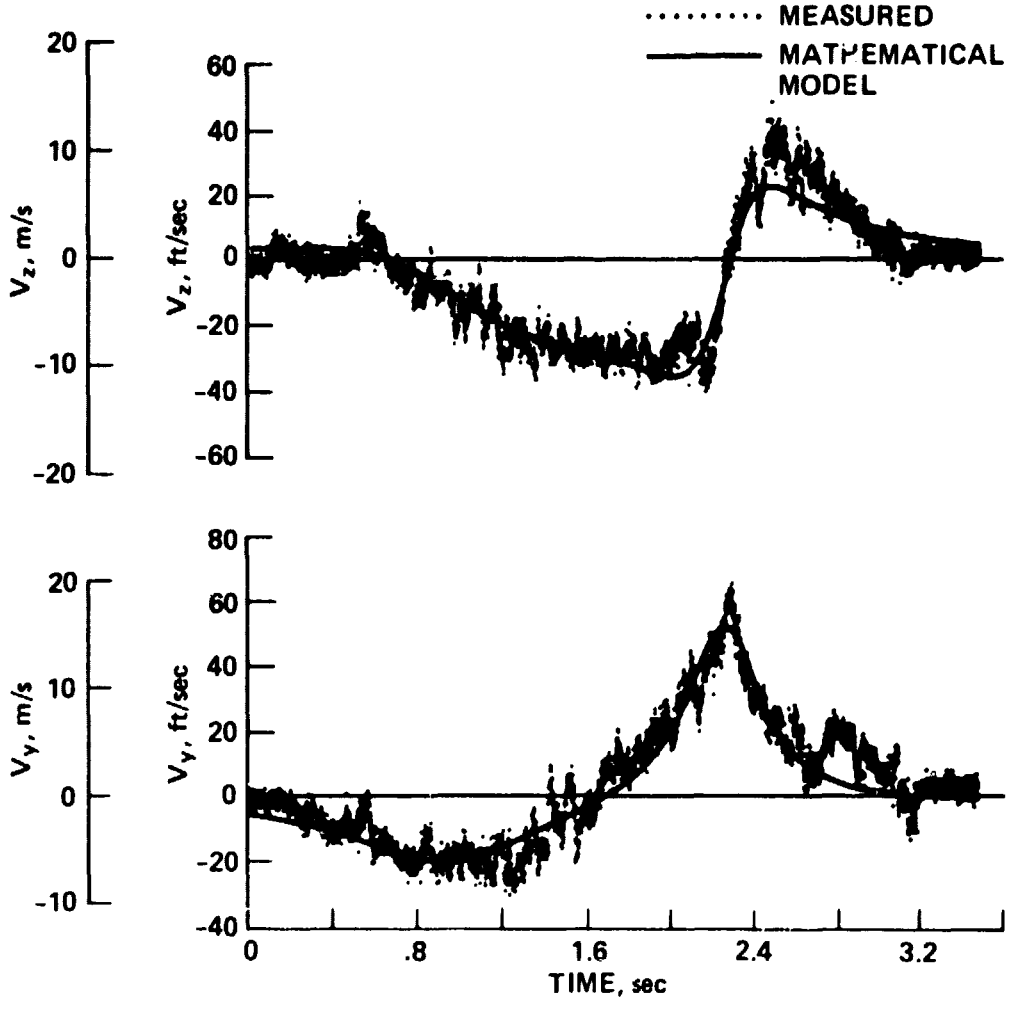

Figure 15.- Velocity profiles for results shown in figure 14.